Enhanced terahertz extinction of single plasmonic antennas with conically tapered waveguides



2013 New J. Phys. 15 015006

(http://iopscience.iop.org/1367-2630/15/1/015006)

New Journal of Physics
The open access journal for physics

# Enhanced terahertz extinction of single plasmonic antennas with conically tapered waveguides

**M C Schaafsma[1,5], H Starmans[1,2], A Berrier[1,4] and J Gómez Rivas[1,3]**

[1] Center for Nanophotonics, FOM Institute AMOLF, c/o Philips Research Laboratories, High Tech Campus 4, 5656 AE Eindhoven, The Netherlands
[2] Optics Research Group, Faculty of Applied Sciences, Delft University of Technology, Lorentzweg 1, 2628 CJ Delft, The Netherlands
[3] COBRA Research Institute, Eindhoven University of Technology, PO Box 513, 5600 MB Eindhoven, The Netherlands
E-mail: m.schaafsma@amolf.nl

*New Journal of Physics* **15** (2013) 015006 (14pp)
Received 22 June 2012
Published 18 January 2013
Online at http://www.njp.org/
doi:10.1088/1367-2630/15/1/015006

**Abstract.** We demonstrate experimentally the resonant extinction of terahertz (THz) radiation by a single plasmonic bowtie antenna, formed by two n-doped Si monomers with a triangular shape and facing apexes. This demonstration is achieved by placing the antenna at the output aperture of a conically tapered waveguide, which enhances the intensity of the incident THz field at the antenna position by a factor of 10. The waveguide also suppresses the background radiation that is otherwise transmitted without being scattered by the antenna. Bowtie antennas, supporting localized surface plasmons, are relevant due to their ability to resonantly enhance the field intensity at the gap separating the two triangular elements. This gap has subwavelength dimensions, which allows the concentration of THz radiation beyond the diffraction limit. The combination of a bowtie plasmonic antenna and a conical waveguide may serve as a platform for far-field THz time-domain spectroscopy of single nanostructures placed in the gap.

[4] Present address: Universität Stuttgart, 1. Physikalisches Institut, Pffafenwaldring 57, 70550 Stuttgart, Germany.
[5] Author to whom any correspondence should be addressed.

## Contents



## 1. Introduction

Terahertz time-domain spectroscopy (THz-TDS) has great potential for the investigation of fundamental transitions in organic and inorganic molecules and nanostructures. Translational and rotational degrees of freedom in polyatomic gases and bio-molecules, lattice vibrations in crystalline structures, conduction electrons in metals and semiconductors, all have resonances at THz frequencies in the range of 0.1–3 THz [1–4]. In typical far-field implementations of THz spectroscopy, the wavelength greatly exceeds the length scale of the individual objects under investigation, e.g. bio-molecules or nanostructures. Therefore, spectroscopy of single objects is challenging and measurements are usually made in large ensembles at high concentrations. When working with a limited amount of material or individual objects, the response may drop below the detection threshold. In order to compensate for these constraints, local field enhancements into subwavelength volumes are needed. Resonant conducting structures, sustaining localized surface plasmon resonances (LSPRs), are key in realizing these large local field enhancements [5–8].

In this paper, we demonstrate that it is possible to detect and measure the extinction of a single bowtie antenna in a standard THz time-domain spectrometer. The antenna is formed by two triangular monomers with facing apexes, separated by a 5 $\mu$m gap. The monomers are made of doped Si with a metallic behavior at THz frequencies [9]. In contrast with metals and perfect electric conductors with vanishing skin depth, the doping level of the silicon used in this work allows for the penetration of the electromagnetic field in the antennas. This finite skin depth gives rise to the plasmonic behavior at THz frequencies [7, 8]. The investigated antenna exhibits an LSPR at around 0.35 THz when excited by a plane wave polarized along its long axis. This resonance is the result of the coherent oscillation of the free charge carriers, harmonically driven by the incident THz electric field. Plasmonic bowtie antennas can locally enhance the field intensity at the LSPR frequency by several orders of magnitude in the gap between the individual monomers. This gap has typically a volume of $\sim 10^{-6}\lambda^3$. The large intensity enhancement in deep subwavelength volumes opens the possibility for THz spectroscopy of single nanostructures or at very low concentrations of material. However, the scattering and extinction cross sections of such a plasmonic antenna can be still small compared to the beam size of the THz pulse in standard THz-TDS setups. To make the detection of a single antenna possible we use a conically tapered waveguide. Tapered waveguides have been proposed to guide and enhance THz radiation into a confined region [10–12]. Zhang and Grischkowsky [13] investigated the adiabatic compression of tapered parallel-plate waveguides, Zhan *et al* [14] showed superfocusing of THz radiation using tapered parallel-plate waveguides and Wächter

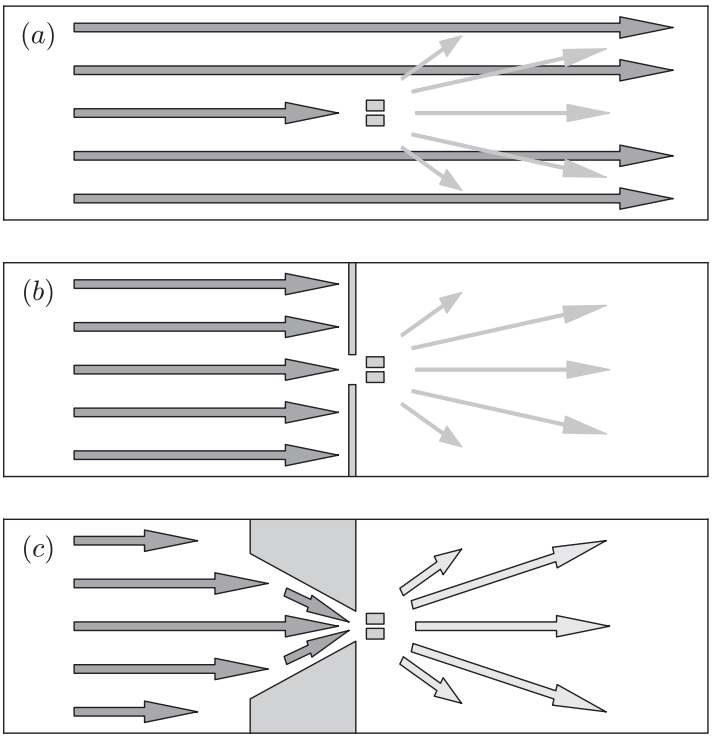


**Figure 1.** Schematic representation of experiments conducted on a single antenna. (a) A plasmonic antenna with a small cross section is illuminated by a spatially extended beam. Only a small fraction of the field is scattered and absorbed by the antenna. In a transmission experiment, there is a large background of unscattered radiation. (b) A cylindrical waveguide or a metallic screen will block this background. However, the incident intensity is also reduced. (c) The enhancement of this intensity is possible by concentrating the incident field on the antenna with a conically tapered waveguide.

*et al* used photoconductive THz field probes for subwavelength imaging [15]. Enhanced THz transmission through conically tapered waveguides was recently reported by Nguyen *et al* [16]. We extend here the application domain of conically tapered waveguides by measuring the extinction of single resonant antennas located at the waveguide output, where the intensity is enhanced.

A schematic diagram of an experiment conducted on a single antenna is shown in figure 1(a). A linearly polarized THz beam is used to illuminate a single plasmonic antenna. Since the antenna has an extinction cross section much smaller than the size of the beam, only a small fraction of the incident field is extinct by scattering and absorption in the antenna. The majority of the field is transmitted as unperturbed by the antenna, leading to a large background in extinction measurements. In order to reduce this background, a thin metallic screen can be used to transmit only the relevant part of the THz beam that interacts with the antenna (figure 1(b)). Although the signal-to-background ratio is improved in this configuration, only a small fraction of the incident beam is used and the signal-to-noise is not increased. To enhance the signal-to-noise, it is possible to use a tapered waveguide. The conical design guides the off-center parts of the field in the direction of the antenna, resulting in an enhanced THz

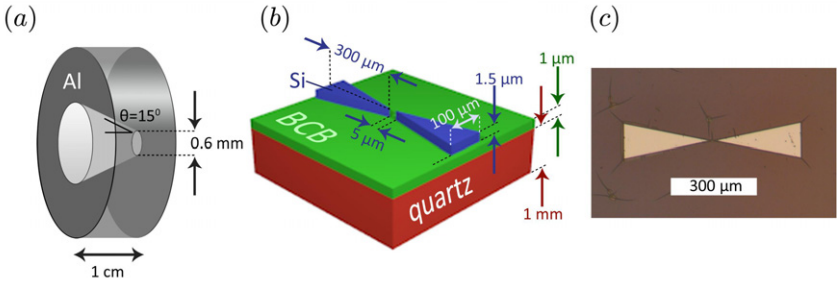


**Figure 2.** Schematic representation of the conical waveguide (a) and the bowtie antenna (b). Optical microscope image of the bowtie antenna (c). The antenna is made of two triangular monomers of n-doped Si, bonded onto a quartz substrate with benzocyclobutene (BCB). The cracks in the microscope image are in the supporting BCB layer.

electromagnetic intensity at the output aperture. This intensity enhancement leads also to an enhanced response of the antenna, allowing a more sensitive spectroscopy.

The paper is organized as follows. The fabrication of the bowtie antenna and waveguides is described in section 2. In section 3, we present simulations of the near field intensity enhancement (FIE) of single bowtie antennas and the conical waveguide, as well as the enhanced intensity transmission of the latter. THz extinction measurements of single THz antennas at the output of the conical waveguide are compared with the extinction of a random array of similar antennas in section 4. These measurements demonstrate the enhanced extinction of single antennas mediated by the enhanced intensity at the output of the waveguide. The paper ends with the conclusions.

## 2. Waveguide and antenna fabrication

Two waveguides have been fabricated for the experiments. A conical shape waveguide is used to enhance the field at its output aperture and a cylindrical waveguide with the same output dimensions is used to reference the transmittance. The waveguides have been fabricated using electrical discharge machining: a conically tapered electrode with a half-angle of 15° is lowered through an aluminum plate of 1 cm thickness, eroding a conical hole. The electrode is lowered until the exit aperture has a diameter of 0.6 mm, leaving an input aperture of 6 mm. A cylindrical waveguide is obtained by lowering an electrode with a diameter of 0.6 mm through a 0.5 mm thick aluminum sheet. These dimensions are chosen such that the intensity enhancement produced by the conically tapered waveguide at its exit aperture is maximum in the frequency range of the plasmonic resonance of the bowtie antennas. The cylindrical waveguide has a finite transmission for frequencies slightly below the cutoff frequency, since evanescent field components can tunnel through the waveguide. When normalizing the conically tapered waveguide by this thin waveguide the value of the intensity enhancement is slightly reduced. However, for this work the slight loss in enhancement is not relevant since the frequencies of interest for the bowtie antenna are above the cutoff frequency.

A schematic representation of the conical waveguide is shown in figure 2(a).

The semiconductor plasmonic antennas have been fabricated using conventional micro-fabrication techniques [17]: a silicon-on-insulator (SOI) wafer with a 1.5 $\mu$m thick undoped

top layer is implanted with arsenic atoms, introducing a free carrier concentration of $(6 \pm 3) \times 10^{19}\,\mathrm{cm}^{-3}$. This doping level produces in silicon a finite conductivity at THz frequencies. The SOI wafer is bonded onto a 1 mm thick quartz substrate with BCB. The silicon substrate and oxide layer are subsequentially removed with wet chemical etching using KOH and HF. The antenna structures are defined using optical lithography and reactive ion etching.

The plasmonic behavior of a semiconductor bowtie antenna is determined by the doping level, and the antenna geometry. The bowtie antenna is formed by two monomers with a triangular shape with a base of 100 $\mu$m, a triangle height of 300 $\mu$m and a monomer height of 1.5 $\mu$m. The triangles have facing apexes, separated by a gap of 5 $\mu$m. As is shown below, this structure has an LSPR around 0.35 THz.

A schematic representation of the bowtie antenna and an optical microscope image are shown in figures 2(b) and (c), respectively. The cracks observed in the image are cracks in the BCB layer. These cracks have a typical width of a micron, being much smaller than the wavelength of THz radiation, and do not influence the measurements.

## 3. Simulations

The local field enhancement of the bowtie antenna and the transmission properties of the conical waveguide are studied using a three-dimensional (3D) finite element method (FEM) in the frequency domain (COMSOL Multiphysics). For the simulations, we use the antenna dimensions determined from the optical image (figure 2(c)). The dielectric properties of the n-doped Si are approximated with the Drude model [18], using parameters given in [19]. Consistent with the experimental results, we use a carrier concentration of $6 \times 10^{19}\,\mathrm{cm}^{-3}$, resulting in a plasma frequency of around 70 THz. For simplicity, we ignore the presence of the substrate in the simulations, assuming that the antenna is homogeneously surrounded by air. Although this simplification might introduce a shift in the LSPR frequency, the underlying physical mechanism will not change.

Figure 3 shows the FIE as a function of frequency, position and polarization. The FIE is defined as the local intensity of the total electromagnetic field divided by the intensity of the incident electromagnetic field. Figures 3(a) and (b) show the maximum FIE in the antenna gap as a function of the frequency of the incident THz radiation. This incident radiation is polarized parallel to the long axis (a) and the short axis (b) of the antenna, respectively.

When driven along the long axis, the free electrons in the semiconductor bowtie antenna resonate around the LSPR frequency. There is a capacitive coupling of the two monomers across the gap. This coupling, arising from the Coulomb attraction of charges across the short distance separating the two monomers, gives rise to an intensity enhancement in the gap. The enhancement is further increased by the lighting-rod effect that results from the sharp tips forming the apex of the triangles. The simulations show an intensity enhancement in the gap over four orders of magnitude under LSPR conditions (figure 3(c)). For an incident polarization along the short axis of the antenna there is no field enhancement relative to the incident field and the spectrum is flat, since for this polarization the antenna is not resonant with the incident THz wave. The FIE in the simulations is maximum at 0.34 THz. The FIE at this frequency in the plane at the middle height of the antennas is shown in figures 3(c) and (d) for the respective polarizations. For the polarization along the long axis (figure 3(c)), the intensity is moderately enhanced in a small region around the bases of the monomers and enhanced significantly in the gap between the two monomers. At certain locations strong suppressions in the intensity

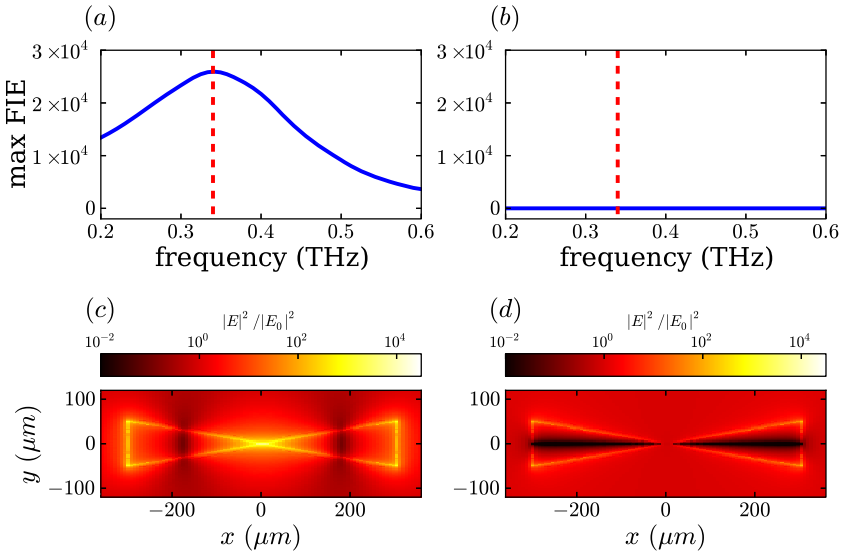


**Figure 3.** 3D FEM simulations of the local FIE of a doped silicon bowtie antenna formed by two triangular monomers for polarizations along the long and the short axis of the antenna, respectively. The antenna is illuminated at normal incidence, i.e. the incident wave vector is normal to the plane of the figure. The antenna dimensions are as discussed in the text. Panel (a) shows the spectrum of the maximum FIE in the gap for the incident THz radiation polarized parallel to the long axis of the antenna, while panel (b) shows the spectrum of the FIE for the incident THz radiation polarized parallel to the short axis of the antenna. Panels (c) and (d) show the FIE in the plane at the middle height of the antenna for the polarizations parallel to the long (c) and short (d) axes at the LSPR frequency, as indicated by the red dashed lines in (a) and (b).

can be observed. The origin of the reduced intensity outside the antenna is due to destructive interference between the incident field and the field scattered by the antenna. Inside the antenna the intensity drops due to the skin depth of the conductor. This drop in intensity is clearly visible in figure 3(d) where the antenna is not at resonance and no significant field enhancement is present. Note that these enhancements might be different in a real sample due to the rounding of the antenna tips and the presence of the substrate. Nevertheless, the simulations illustrate that resonant bowtie antennas are capable of focusing and enhancing locally electromagnetic fields in subwavelength volumes.

The transmission properties of the conically tapered and cylindrical waveguides are simulated using the FEM (COMSOL) and finite-difference in time domain (FDTD, CST Microwave Studio) techniques. As sketched in figure 1, a linearly polarized plane wave travels from left to right through the system. The dimensions of the waveguides used for the simulations are those described in section 2, i.e. both waveguides having an output aperture of 0.6 mm diameter, and the conically tapered waveguide having an input aperture of 6.0 mm diameter. The aluminum forming the waveguides is simulated as a perfect electric conductor. For the FDTD simulations a broadband Gaussian pulse is sent through the system, and the intensity of the transmitted field is monitored behind the waveguide. The simulated time domain signals are Fourier transformed and squared, resulting in the power spectrum of transmitted intensities.

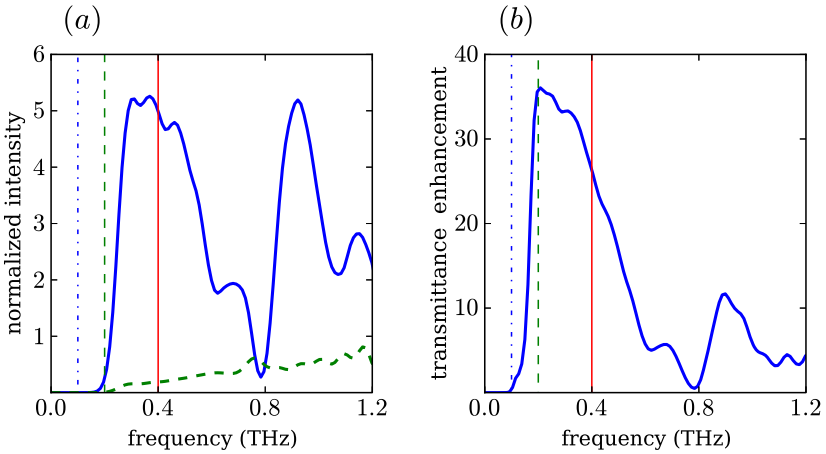


**Figure 4.** (a) Simulated intensity spectra of a conically tapered (blue solid) and a cylindrical (green dashed) waveguide at a distance of 1 mm after the output aperture, normalized to the incident intensity. (b) Transmitted intensity of the conically tapered waveguide referenced by the cylindrical waveguide. The vertical lines in both figures correspond to the frequencies at which the intensity enhancements are shown in figure 5.

Figure 4(a) shows the intensity spectrum, defined as the intensity at 1.0 mm after the waveguide, normalized by the intensity incident on the waveguide. It is important to note that the normalized intensity is strongly dependent on the distance to the output aperture. At short distances, evanescent field components will give larger field intensities whereas when the distance is increased the intensity decreases roughly with the inverse of the square of the distance due to diffraction. The spectrum of the conically tapered waveguide is indicated with the blue solid curve, and the cylindrical waveguide with the green dashed curve. At low frequencies the transmittance vanishes. These frequencies are below the cutoff frequency defined by the output aperture of the waveguides. For an infinitely long cylindrical waveguide with a diameter of 0.6 mm the cutoff frequency is 0.3 THz [20].

Figure 4(b) shows the intensity transmittance enhancement, which is defined as the transmittance through the conically tapered waveguide normalized by the transmittance through the cylindrical waveguide. The conically tapered waveguide enhances the transmitted field intensity, while the cylindrical waveguide only transmits a fraction of the intensity incident onto the opening, reflecting the rest. The conically tapered waveguide guides the incident field at the larger input aperture towards the smaller output aperture. These fields travel a longer distance, picking up an additional phase compared to the direct transmitted fields. For the given waveguide dimensions this results in destructive interference and a minimum in the transmitted intensity around 0.8 THz. For a perfect adiabatic transmission through a tapered waveguide, the FIE at the output aperture is given by the ratio of the input to output aperture cross sections. This ratio is 100 for the conically tapered waveguide used here. However, the transmission is not adiabatic due to a too large tapering angle and the field experiences reflections as it propagates through the waveguide. Therefore, the simulated intensity enhancement of the conically tapered waveguide over the cylindrical waveguide reaches a value of around 35.

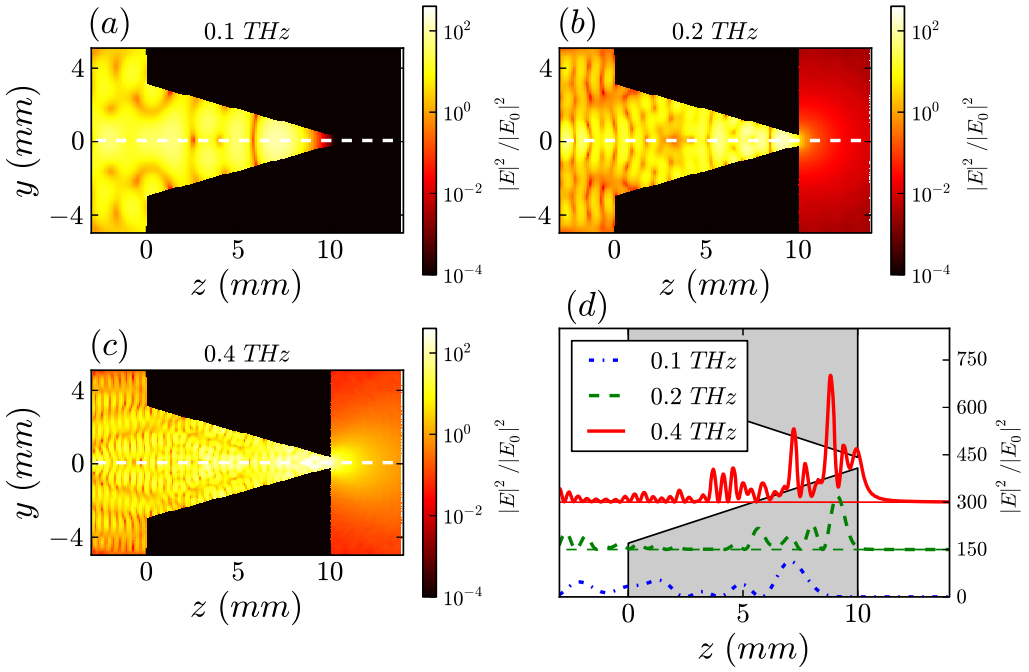


**Figure 5.** Simulations of the intensity enhancement of the THz electromagnetic field propagating through a conically tapered waveguide at various frequencies. A linearly $y$-polarized plane wave enters the waveguide from the left and travels to the right. 2D cuts through the center of the waveguide are shown for frequencies of 0.1 THz (a), 0.2 THz (b) and 0.4 THz (c). These frequencies correspond to frequencies below, around and above the cutoff frequency of the waveguide, respectively. Line cuts of the total FIE through the center of the waveguide along the direction of propagation of the wave are shown in (d). For clarity, the field intensities at 0.2 and 0.4 THz have been vertically displaced.

Figure 5 shows FEM simulations for the total FIE in the conically tapered waveguide. A monochromatic and linearly $y$-polarized plane wave propagates from left to right. The total intensity enhancement in the plane through the center of the waveguide along the polarization direction—the $yz$-plane—is shown for frequencies below (figure 5(a)), around (b) and above (c) the cutoff. Cuts through these maps along the dashed white lines are shown in figure 5(d). For frequencies below the cutoff there is an enhancement of the field inside the waveguide, but the transmitted intensity is reduced because the propagating field is fully reflected before the output aperture is reached. The interference pattern in the intensity enhancement is the result of the interference of the incident field and this reflection. For waves having frequencies close to the cutoff frequency, there is a transition from the evanescent transmitted field to propagating waves. Figure 5(b) shows that although most of the wave is reflected a small fraction is transmitted. For frequencies well above the cutoff, figure 5(c), the field propagates through the waveguide. This condition is needed for a maximum enhancement of the transmission. We note that even for this frequency, significant reflection takes place and the interference pattern is formed. This reflection can be minimized by reducing the tapering angle of the waveguide in order to allow an adiabatic focusing of the incident THz field onto the output aperture [10].

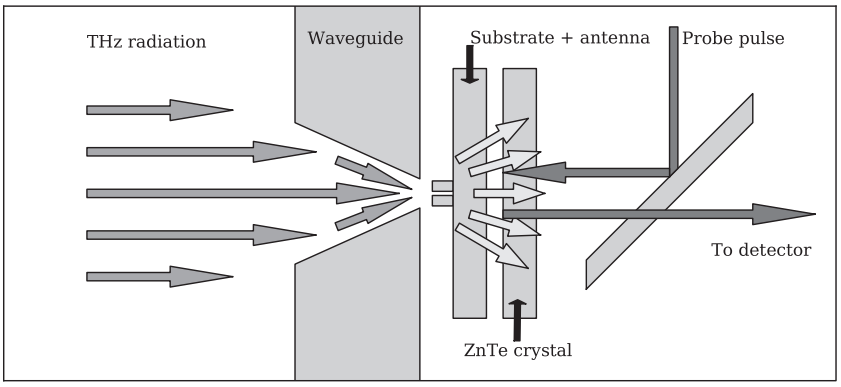


**Figure 6.** Schematic illustration of the experimental setup for detecting a single plasmonic antenna. The waveguide is placed in the focus of the THz beam, in front of the ZnTe crystal. The substrate with the antenna is placed in direct contact with the waveguide. The THz radiation travels through the waveguide, passes the antenna and substrate and propagates through the ZnTe crystal. From the opposite direction the IR probe pulse reflects on the left face of the ZnTe crystal, probing on its way back the THz electric field, after which it is directed to the detector. The illustration is not to scale.

## 4. Terahertz transmission and extinction measurements

The THz transmission experiments were carried out with a standard THz-TDS setup [3]. A Ti:sapphire oscillator (Femtolasers, Fusion 20-800) generates a 75 MHz train of 20 fs near-infrared (NIR) pulses with a wavelength around 800 nm. Using a beam splitter, each pulse is split into two. One pulse is used to generate a broadband and linearly polarized THz pulse in a GaAs photoconductive antenna (Gigaoptics, TeraSED). The resulting THz beam is guided through the setup using off-axis parabolic mirrors, and focused onto a ZnTe crystal. The THz electromagnetic field is probed in this crystal utilizing the electro-optic effect. The second NIR pulse from the beam splitter travels through the ZnTe crystal, co-propagating with the THz in space and with a well-controlled delay in time. Since the duration of the NIR pulse is very short compared to the THz pulse (20 fs versus 2 ps), the NIR pulse will only overlap with a small portion of the THz pulse in which the amplitude of the THz can be considered constant. This amplitude induces in the ZnTe crystal a proportional change in the polarization state of the NIR pulse, which change can be detected. By scanning the time delay between the two pulses, the full time-domain signal of the THz transient can be acquired. Using a knife-edge technique the spatial profile of the cross section of the focused THz beam has been verified as Gaussian, with a full-width at half-maximum of 1.7 mm.

The THz beam, having traveled through the waveguide, becomes highly divergent. In order to optimize the co-propagation of the two pulses, the waveguide is placed close to the ZnTe crystal. Since one of the sides of the ZnTe crystal is obstructed by the waveguide, the probe pulse is coupled from the back side, reflecting on the front face of the ZnTe crystal after which it can probe the THz electric field. This reflection is directed to the detector for analysis. A schematic representation of the detection scheme is displayed in figure 6. It is worth noting that THz-TDS detects the amplitude of the THz electric field as a function of time

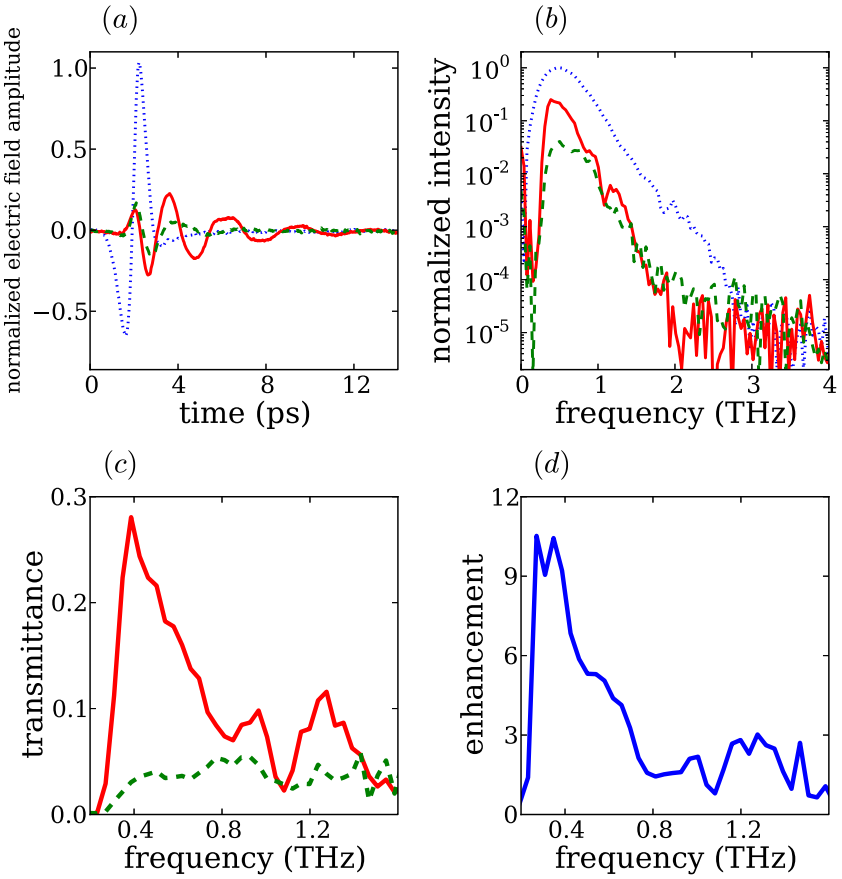


**Figure 7.** Experimental characterization of the conically tapered and cylindrical waveguides. (a) Time-domain transmission measurements of the reference (blue dotted), conically tapered (red solid) and cylindrical (green dashed) waveguides. (b) Intensity spectra of the time-domain signals shown in (a). (c) Transmitted intensity spectra of the conically tapered (red solid) and cylindrical (green dashed) waveguides normalized by the free space reference. (d) Transmittance enhancement of the conically tapered waveguide, defined as the transmittance through this waveguide normalized by the transmittance through the cylindrical waveguide.

(THz transients). The amplitude transients can be Fourier transformed to obtain the amplitude spectra, which can be squared to obtain the power spectra. The power spectra are proportional to the THz intensity. In the analysis done below we determine the power spectra and the intensity transmittance from the THz transients.

The experimental characterization of the conically tapered and cylindrical waveguides is shown in figure 7. Both waveguides are measured in transmission and compared against each other and a reference measurement taken without a waveguide, i.e. the response function of the setup. The time-domain signals (figure 7(a)) show that the presence of the cylindrical waveguide severely reduces the transmitted signal, since most of the incident amplitude is blocked by the waveguide. The enhanced amplitude transmission of the conically tapered waveguide, relative to the cylindrical waveguide, is visible as an increase in the THz pulse dispersion. This is the

contribution of the field that illuminated the entrance of the waveguide at a larger radius, and has picked up an additional phase before reaching the output aperture.

The intensity spectra are shown in figure 7(b), and are the square of the Fourier transform of the time-domain signals, after zero padding. The intensity is normalized against the maximum of the setup response. For the empty setup (blue-dotted curve) the noise floor is reached around 3 THz and the maximum signal-to-noise spans five orders of magnitude. Both the conical (red solid curve) and cylindrical (green dashed curve) waveguides reduce the bandwidth to about 2 THz. The enhancement of the conical waveguide over the cylindrical waveguide is clearly visible in the range of 0.3–0.8 THz. The intensity transmittance spectra for the conically tapered (red solid curve) and cylindrical (green dashed curve) waveguides in figure 7(c) are obtained by normalizing the spectra shown in figure 7(b) against the setup response, i.e. the intensity spectrum measured without any waveguide. For both waveguides the transmittance vanishes at the lowest frequencies due to cutoff. The transmittance remains below 0.05 for the cylindrical waveguide even at higher frequencies. This reduced intensity transmittance is due to the large area of the incident beam that is blocked. In our setup, roughly 95% of the energy carried by the THz beam is contained in an area of 8 $mm^2$, while the area of the aperture of the cylindrical waveguide is 0.3 $mm^2$. This ratio of 1/25 matches the experimental results. The transmittance is enhanced for the conical waveguide, compared to the cylindrical one.

The same spectral dependence of the simulated intensity of figure 4(a) is observed in the transmittance spectra shown in figure 7(c), with a maximum in the intensity and transmittance of the conical waveguide at 0.4 THz. The transmittance approaches 0.3 at 0.4 THz, while the output aperture only encloses around 5% of the area of the incident pulse. Note that the simulations in figure 4(a) refer to the intensity at the output aperture normalized to the incident intensity in an equivalent area at the input aperture of the waveguide, while the transmittance of figure 7(c) represents the total intensity incident onto the input aperture being transmitted through the waveguide. Therefore, the vertical scales of figures 4(a) and 7(c) should not be directly compared.

The reduced intensity transmittance around 1.0 THz is also consistent with the simulations, and can be explained by the aforementioned destructive interference in the wavefront. The blue shift of this minimum in the measurements, compared to the simulations, can be attributed to the approximation of plane wave illumination used for the simulations. In the simulations, the complete input aperture is illuminated by a plane wave, whereas in the experiments the pulse has a Gaussian profile and is slightly smaller than the input aperture of the waveguide. This smaller size of the beam reduces the effective height of the waveguide and introduces a blue shift of the interference features. Figure 7(d) displays the intensity transmittance of the conically tapered waveguide normalized by the cylindrical waveguide, showing the enhancement of the transmittance of the conically tapered waveguide over the complete range of 0.1–1.4 THz. The maximum intensity enhancement is around one order of magnitude at 0.4 THz. As the cylindrical waveguide should not enhance the intensity, the enhancement of the conical waveguide should be the same when compared to the incident field.

A single bowtie antenna is placed directly at the output aperture of the conically tapered waveguide, as shown in the inset of figure 8(a). The measured extinction, which is defined as 1 minus the intensity transmittance, of this single antenna in front of the waveguide is shown in figure 8(a) with the red solid curve. The transmission measurements through the single antenna are referenced to the transmission of the waveguide with an empty quartz substrate at the output entrance, i.e. without the antenna. A resonance is clearly resolved in this measurement

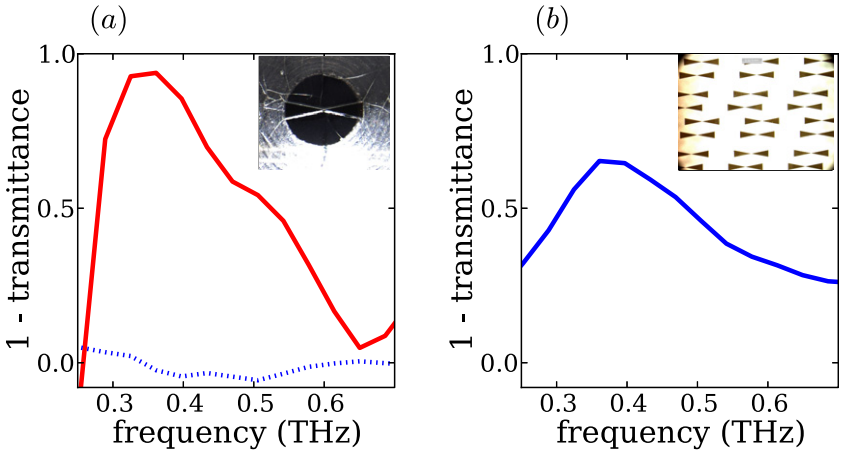


**Figure 8.** Extinction measurements of bowtie antennas, illuminated with a polarization along the long axis and referenced against an empty quartz substrate. (a) The extinction spectra of a single bowtie antenna measured with the conically tapered waveguide (red solid) and without any waveguide (blue dotted). In the inset an optical microscope image of the antenna mounted in front of the conically tapered waveguide is shown. (b) The extinction of a random array of close packed antennas; the inset contains an optical microscope image of the array.

with a maximum extinction of 90% around 0.35 THz. This enhanced extinction corresponds to the excitation of an LSPR in the plasmonic antenna, which should lead to a large local field enhancement in the bowtie gap. The blue dashed curve in figure 8(a) corresponds to the extinction of the single antenna measured without the waveguide. The response is practically flat and the LSPR cannot be resolved, since the extinction is below the noise level.

To rule out any possible artifact in the measurements that could lead to an extinction peak similar to our measurements, we have confirmed the resonant response of the bowtie antenna by measuring the extinction of a random array of similar antennas without the conically tapered waveguide. An optical microscope image of the sample is shown in the inset of figure 8(b). In this measurement, the THz beam illuminates approximately 30 antennas. Therefore, the extinction is enhanced in this sample by increasing the density of antennas, rather than by concentrating the THz beam with the conical waveguide. A similar extinction spectrum to the single antenna is measured for the random array (figure 8(b)). The extinction reaches a maximum at 0.35 THz, with a resonant response that can be attributed to the excitation of LSPRs.

Surprisingly, there is excellent agreement between the resonant frequency measured in extinction of the bowtie antennas on a quartz substrate and the simulated frequency of maximum FIE in the gap of the antenna homogeneously surrounded by air. In principle, one should expect a shift of the resonance frequency due to the presence of the substrate. The reason why we do not see this shift might be due to the fact that the simulations refer to the near field and that the measurements probe the far-field extinction [21]. Another reason might be deviations of the geometry of the real sample from the simulated structure due to, e.g., rounded tips/corners and underetching of the substrate. The antennas have strong polarization-dependent scattering

properties. Experiments (not shown here) were carried out also for the antennas aligned with the polarization of the incident field along the short axis. These experiments show flat spectra due to the absence of any plasmonic resonance, in agreement with the results shown in figure 3.

The demonstration of the enhanced extinction by a single bowtie antenna opens a range of possibilities for THz spectroscopy of nanostructures or of molecules at low concentrations. For example, the positioning of a nanostructure in the subwavelength gap defined by the two monomers, in which the field is locally enhanced, will enable us to increase the THz field–matter interaction to a level at which far-field spectroscopy of single nanostructures at THz frequencies might be possible.

## 5. Conclusion

We have experimentally demonstrated that a conically tapered waveguide can be used to funnel and enhance the THz intensity. This intensity enhancement allows us to measure the extinction of a single THz plasmonic bowtie antenna, which otherwise cannot be detected due to the large background of unscattered radiation. The transmittance properties were also investigated numerically, revealing excellent agreement with the measurements. The large localized field enhancements that can be achieved by bowtie antennas in subwavelength volumes may open up the possibility of using standard far-field THz time-domain spectrometers for the detection and spectroscopy of single nanostructures.

## Acknowledgments

This work is part of the research programme of the Foundation for Fundamental Research on Matter (FOM), which is part of the Netherlands Organisation for Scientific Research (NWO). The work was partially supported by the European Community's 7th Framework Programme under grant agreement FP7-224189 (the ULTRA project).

## References

[1] Ferguson B and Zhang X C 2002 Materials for terahertz science and technology *Nature Mater.* **1** 26–32
[2] Tonouchi M 2007 Cutting-edge terahertz technology *Nature Photon.* **1** 97–105
[3] Dexheimer S L (ed) 2007 *Terahertz Spectroscopy: Principles and Applications* (*Optical Science and Engineering Series* vol 131) (Boca Raton, FL: CRC)
[4] Jepsen P U, Cooke D G and Koch M 2011 Terahertz spectroscopy and imaging—modern techniques and applications *Laser Phot. Rev.* **5** 124–66
[5] Shi X, Cleary A, Khalid A and Cumming D R S 2009 Multiple plasmon resonances at terahertz frequencies from arrays of arsenic doped silicon dots *Microelectron. Eng.* **86** 1111–3
[6] Tian Z, Azad A K, Lu X, Gu J, Han J, Xing Q, Taylor A J, O'Hara J F and Zhang W 2010 Large dynamic resonance transition between surface plasmon and localized surface plasmon modes *Opt. Express* **18** 12482–8
[7] Berrier A, Ulbricht R, Bonn M and Gómez Rivas J 2010 Ultrafast active control of localized surface plasmon resonances in silicon bowtie antennas *Opt. Express* **18** 23226–35
[8] Giannini V, Berrier A, Maier S A, Sanchez-Gil J A and Gómez Rivas J 2010 Scattering efficiency and near field enhancement of active semiconductor plasmonic antennas at terahertz frequencies *Opt. Express* **18** 2797–807

[9] Saxler J, Gómez Rivas J, Janke C, Pellemans H P M, Haring Bolivar P and Kurz H 2004 Time-domain measurements of surface plasmon polaritons in the terahertz frequency range *Phys. Rev.* B **69** 155427
[10] Rusina A, Durach M, Nelson K A and Stockman M I 2008 Nanoconcentration of terahertz radiation in plasmonic waveguides *Opt. Express* **23** 18576–89
[11] Kim S-H, Lee E S, Ji Y B and Jeon T I 2010 Improvement of THz coupling using a tapered parallel-plate waveguide *Opt. Express* **18** 1289–95
[12] Zon V B and Zon B A 2011 Terahertz surface plasmon polaritons on a conductive right circular cone: analytical description and experimental verification *Phys. Rev.* A **84** 013816
[13] Zhang J and Grischkowsky H 2005 Adiabatic compression of parallel-plate metal waveguides for sensitivity enhancement of waveguide THz time-domain spectroscopy *Appl. Phys. Lett.* **86** 061109
[14] Zhan H, Mendis R and Mittleman D M 2010 Superfocusing terahertz waves below $\lambda/250$ using plasmonic parallel-plate waveguides *Opt. Express* **18** 9643–50
[15] Wächter M, Nagel M and Kurz H 2009 Tapered photoconductive terahertz field probe tip with subwavelength spatial resolution *Appl. Phys. Lett.* **95** 041112
[16] Nguyen T D, Vardeny Z V and Nahata A 2010 Concentration of terahertz radiation through a conically tapered aperture *Opt. Express* **18** 25441–8
[17] Berrier A, Albella P, Ameen Poyli M, Ulbricht R, Bonn M, Aizpurua J and Gómez Rivas J 2012 Detection of deep-subwavelength dielectric layers at terahertz frequencies using semiconductor plasmonic resonators *Opt. Express* **20** 5052–60
[18] Ashcroft N W and Mermin N D 1976 *Solid State Physics* (Philadelphia, PA: Saunders)
[19] Adachi S 2004 *Handbook on Physical Properties of Semiconductors* vol 1 (Boston, MA: Kluwer Academic)
[20] Marcovitz N 1951 *Waveguide Handbook* (Lexington, MA: Boston Technical Publishers)
[21] Messinger B J, Von Raben K U, Chang R K and Barber P W 1981 Local fields at the surface of noble-metal microspheres *Phys. Rev.* B **24** 649–57